

Long-Term Operation of Perovskite-Catalyzed Bifunctional Air Electrodes in Rechargeable Zinc-Air Flow Batteries

Birgit Pichler,^{*[a]} Kurt Mayer,^[a] and Viktor Hacker^[a]

Rechargeable zinc-air flow batteries are investigated as promising stationary energy storage system due to compact system design and low cost materials. Bifunctional air electrodes employing a $\text{La}_{0.6}\text{Sr}_{0.4}\text{Co}_{0.2}\text{Fe}_{0.8}\text{O}_3$ perovskite catalyst for O_2 -reduction and O_2 -evolution are manufactured in small scale (4 cm^2) and in up-scaled sizes ($50\text{--}55 \text{ cm}^2$) and tested in unit cell configuration with flowing electrolyte. Stable operation of 1000 h is achieved in the small set-up with an overall 1800 h of operation over 700 cycles at high voltage efficiencies of $>50\%$

(air electrode) at 50 mA cm^{-2} . The up-scaled flow cell reaches nearly the same performance for 320 h and 130 h, respectively, proving the successful scale-up. Slowly decreasing hydrophobicity is found to be the main reason of initially increasing but then decreasing performance. This is confirmed by electrochemical impedance spectroscopy. Although many problems are suppressed with flowing electrolyte, zinc morphology proves to be the major challenge especially in larger cells in long-term operation of a few hundred hours.

1. Introduction

Fast and inexpensive storage of electrical energy generated by intermittent sources is becoming more and more relevant due to increasing installation capacities of wind and solar power systems.^[1-3] Stationary flow batteries either using fully soluble redox couples (e.g. all-vanadium) or zinc-based hybrid systems (e.g. Zn-Br_2) have been developed with low costs as an important goal with the DOE target for stationary energy storage being below 150 \$US per kWh.^[4-9] Metal-air cell configurations, using for example zinc as the abundant and low cost ($\sim 2 \text{ $US per kg}$ ^[7]) active storing metal, are thereby of increasing interest as summarized in recent review publications.^[10-15] When flow-assisted (i.e. zinc-air flow battery, ZAFB), these hybrid systems are regarded as "next-generation" flow battery^[12] due to compact system design with only one low cost electrolyte ($\sim 4 \text{ $US kWh}^{-1}$ ^[7]) and one external tank containing the metal zinc in form of zincate (instead of ZnO as in stationary batteries). Also, there is no need for costly separators or anion exchange membranes.^[7] The energy density of the hybrid system is limited by the amount of zinc storable as zincate in alkaline solution ($\sim 0.8 \text{ M}$ in 8.2 M (35 wt%) KOH)^[11] on the one hand and on the other hand by the area of the zinc electrode.^[7] A detailed analysis of a large-scale demonstration

ZAFB was recently published by Amunatgeui et al.,^[16] who concluded that this system is mainly suited for low power and long duration energy storage.

Zinc-air flow batteries employ a bifunctional air electrode for oxygen reduction reaction (ORR) in discharge mode and for oxygen evolution reaction (OER) during charging, thus electrochemically converting freely available oxygen from the ambient air. So far, mainly three-electrode configurations using a separate charge and discharge air electrode have been employed,^[16-18] nevertheless, the two-electrode configuration with one zinc electrode and only one air electrode would be preferred because of the more compact cell design and the easier handling of the electrical circuitry.^[16]

Numerous catalysts with high activity have been reported in literature to be able to bifunctionally catalyze ORR and OER, but activity measurements are often performed ex-situ by means of cyclic voltammetry using rotating ring disk electrodes or demonstrated with shorter in-situ tests of about 100 h (compare to Table S1 in the supporting information). Thereby long-term stability and degradation mechanisms are often less studied. The bifunctional catalysts for alkaline media can be classified^[10] as i) precious metal (e.g. Pt and IrO_2 , commonly utilized for benchmarking but not really bifunctional^[13]), ii) transition metal oxide catalysts,^[19] such as spinels (AB_2O_4)^[20] and perovskites (ABO_3), but also single metal oxides (NiO_x , CoO_x , MnO_x)^[21] and iii) carbon-based materials for example carbon nanotubes and (reduced) graphene oxide.^[10] Many different perovskite catalysts^[19,22-24] have been investigated, whereby the B-site is generally regarded as the active site. In addition, the doping with heteroatoms has a high impact on catalytic activity as well as on the stability during potential cycling.^[24]

A few alkaline zinc-air flow battery systems have been reported,^[16,17,25-27] but more work needs to be done in regard to implementation of the abovementioned catalysts into stable electrode structures for achieving operation times of hundreds of hours. Nevertheless, by utilizing a flowing electrolyte, common problems of static zinc-air batteries can be reduced,

[a] B. Pichler, K. Mayer, Prof. V. Hacker
Institute of Chemical Engineering and Environmental Technology
Graz University of Technology
Inffeldgasse 25 C, 8010 Graz, Austria
E-mail: birgit.pichler@tugraz.at
kurt.mayer@tugraz.at
viktor.hacker@tugraz.at

 Supporting information for this article is available on the WWW under <https://doi.org/10.1002/batt.201800094>

 An invited contribution to a Special Issue on Bifunctional Catalysts for Metal-Air Batteries

 © 2018 The Authors. Published by Wiley-VCH Verlag GmbH & Co. KGaA. This is an open access article under the terms of the Creative Commons Attribution License, which permits use, distribution and reproduction in any medium, provided the original work is properly cited.

mainly on the zinc electrode by suppressing dendrite growth, shape change and passivation due to a more even zinc distribution and lower concentration gradients. Thus, operation at increased current densities is possible.^[7] Obtaining compact zinc morphologies can further be enhanced by applying pulsating currents during charging.^[28–30] Nevertheless, reduced cycle life, either caused by air electrode degradation or by irreversible changes on the zinc electrode, especially in up-scaled cells, is still a major hindrance for bringing the zinc-air (flow) battery closer to application.

In this work we present durable bifunctional air electrodes manufactured via a scalable process for application in flow-assisted zinc-air batteries. The electrodes employed commercial $\text{La}_{0.6}\text{Sr}_{0.4}\text{Co}_{0.2}\text{Fe}_{0.8}\text{O}_3$ perovskite as catalyst,^[22,23] which allowed more reproducible optimization of the electrode build. Thus, the straightforward manufacturing process also allows easy implementation and characterization of other types of (oxide) catalysts. So far, there are no standardized characterization procedures for zinc-air batteries, also because it usually depends on the focus of the study, e.g. testing of zinc electrodes is often performed with capacity dependent cycles. In this work, the air electrodes were tested at a comparatively high but for stationary systems practically applicable^[5] current density of 50 mA cm^{-2} and long cycle times ($\geq 2 \text{ h}$) in a small 4 cm^2 set-up and in a bigger cell with 50 cm^2 . Insight on degradation mechanisms was gained by electrochemical impedance spectroscopy. Although full unit cells were tested, this work focused its investigations and optimizations regarding longevity and catalytic activity on the bifunctional air electrode.

2. Results and Discussion

2.1. Electrode Manufacture

Bifunctional air electrodes for ORR and OER were manufactured via an easily scalable ($4\text{--}55 \text{ cm}^2$)^[29] manufacturing process, employing a $\text{La}_{0.6}\text{Sr}_{0.4}\text{Co}_{0.2}\text{Fe}_{0.8}\text{O}_3$ perovskite as catalyst in this work. However, the process can be readily adapted for implementation of other catalysts. Nickel foam was utilized as current collector material as it provides good stability and flexibility to the electrode build. By using two separate electrode pastes containing the catalyst – one on each side of the nickel foam – the electrochemical activity of the electrode toward OER on the electrolyte side (two-phase zones between electrolyte and catalyst) and toward ORR on the air supplied side (three-phase boundaries between oxygen/catalyst/electrolyte required) was optimized separately. OER activity, for example, was much enhanced by the addition of fine nickel powder on the electrolyte facing side as the $\text{Ni(OH)}_2/\text{NiOOH}$ redox couple worked as reaction promoting mediator.^[12] Thereby, nickel got repeatedly oxidized/reduced, i.e., during cycling always oxidation/reduction of the $\text{Ni(OH)}_2/\text{NiOOH}$ redox couple took place before ORR/OER (two-step reaction) as was recently studied by Cano et al.^[31] The beneficial effect on the OER performance through the addition of fine Ni powder was also apparent by the lower charging potentials of these electrodes

compared to previously investigated $\text{La}_{0.6}\text{Sr}_{0.4}\text{Co}_{0.2}\text{Fe}_{0.8}\text{O}_3$ perovskite-only air electrodes.^[32]

In the electrode build, an optimized amount of PTFE was utilized as hydrophobic binder material and the added carbon nanofibers (CNF) provided good oxygen accessibility and electrical conductivity by forming a fibrous electrically conductive network. Although less defined and homogenous than carbon nanotubes, the comparatively low-cost CNF had the benefit to exhibit good stability at high anodic potentials compared to other common carbon-type electrode additives such as Vulcan XC72 due to higher graphitized regions.^[24] Although carbon-free electrodes have been developed, for example by Li et al.,^[33] in order to prevent degradation by carbon corrosion, carbon-materials exhibit a synergistic ORR promoting effect especially together with lowly electrically conductive perovskite.^[24] Thus, the discharge performance of the air electrode is significantly enhanced.

Regarding the zinc electrode, in the small test cell a zinc plate (together with air electrode 1, E1) was utilized to ensure sufficient zinc availability on the zinc electrode. In the larger cell, a copper plate coated with a thin layer of pre-deposited zinc (with air electrode 2, E2) was employed in order to prevent contact losses at the clamping. However, Cu in contact with electrolyte was prone to oxidation/reduction during cycling thus proving to be unpractical in this regard, so that in the third cell in combination with air electrode E3, a copper wire, which was soldered onto the backside of a zinc plate, was utilized as current collector. For achieving compact zinc morphologies and for reducing dendrite formation, pulse interrupt currents were applied during charging, thus prolonging the cycle life of the zinc electrode without the addition of modifying additives into the electrolyte.

2.2. Electrochemical Characterization of 4 cm^2 Air Electrode E1

The electrochemical characterization results of a unit cell zinc-air flow battery with 4 cm^2 sized air electrode (E1) is shown in Figure 1, which depicts the air electrode potential and the zinc potential vs. Zn/Zn^{2+} as well as the cell voltage every few hundred hours of testing. The performance of the air electrode alone is depicted in more detail in Figure 2. As can be seen in Figure 1, stable air electrode potentials in the range of 1.0 V (discharge) and 2.0 V vs. Zn/Zn^{2+} (during pulse charging indicated by the thick bars) were achieved between 100 h and 1000 h of operation. Overall, it was possible to charge/discharge cycle the air electrode for 1820 h (i.e., over 800 cycles) until the lower cut-off potential of 0.5 V vs. Zn/Zn^{2+} was reached. Including shut-off times, where the air electrode was kept in static electrolyte and continuously fed with low air flow, the air electrode was mounted in the set-up for 136 days (about 4.5 months).

During the whole operation time (except the first 50 h), the charging potentials of the air electrode were stable between 1.93–1.95 V vs. Zn/Zn^{2+} during the 100 mA cm^{-2} pulse and 1.87–1.89 V vs. Zn/Zn^{2+} during pause (no current), showing

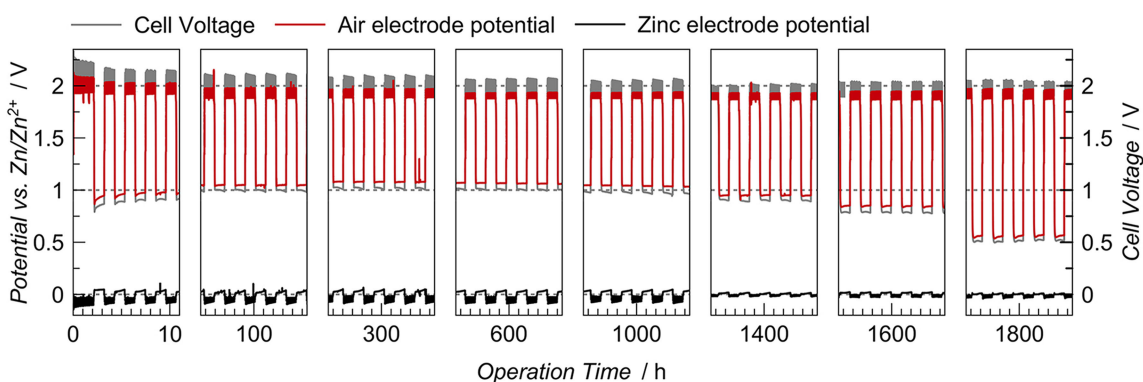


Figure 1. Electrochemical long-term charge/discharge cycling of a zinc-air flow cell with 4 cm^2 bifunctional air electrode (E1) operated at 50 mA cm^{-2} (air) with pulse charging, actively supplied with air at RT and with flowing $8\text{ M KOH} + 0.5\text{ M ZnO}$ electrolyte (8 cm s^{-1} surface flow velocity). Besides cell voltage (right y-axis) the air and the zinc electrode's potentials were separately recorded against Zn/Zn^{2+} reference (left y-axis).

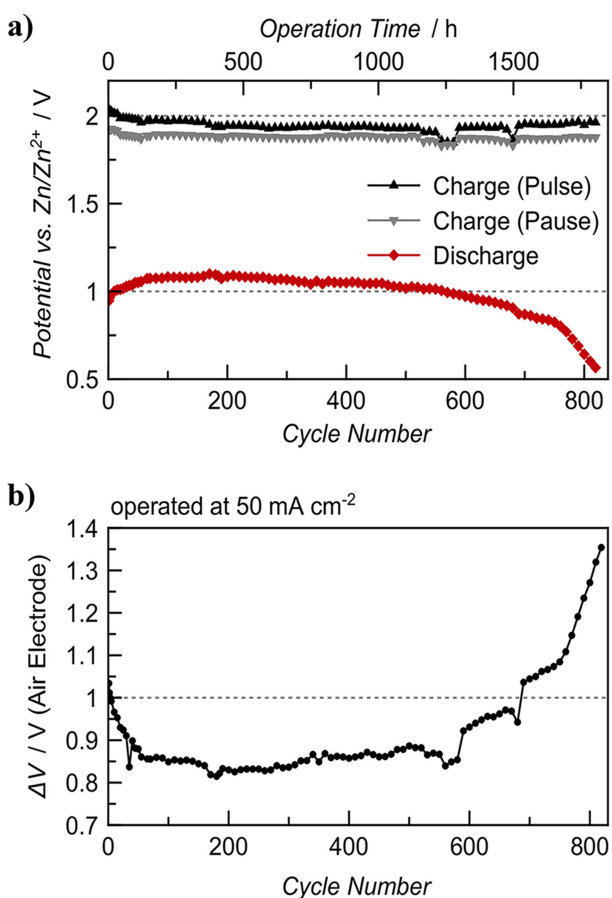


Figure 2. Potential course of the air electrode E1 during long-term operation, a) showing the maximum and minimum potentials during pulse charging (100 mA cm^{-2} pulse for 50 ms, 50 ms pause) and the ORR potentials during discharge and b) the ΔV between charge (mean value) and discharge.

that the OER two-phase zones between catalyst and electrolyte were constant during operation and that product oxygen was effectively removed from the electrode's surface with the flowing electrolyte. The potential difference between charge and discharge of the air electrode (ΔV) was below 1.0 V for 700 cycles and even as low as 0.82 V after 200 cycles (depicted in

Figure 2b), which corresponds to a voltage efficiency of 57% (air electrode only). A detailed list of the potentials and ΔV obtained with this cell is listed in Table S2 in the supporting information.

At the beginning of operation, zinc was pre-deposited by pulse charging onto the zinc electrode from the dissolved ZnO containing electrolyte (first inlet in Figure 1), and the procedure repeated from time to time to prevent zinc depletion over time. Nevertheless, after 1050 h of continuous operation, no zinc was left of the initial 4 cm^2 sized zinc plate, which is attributed to uneven current distribution during deposition, as well as unbalanced charge/discharge capacities.^[11] In consequence, a new, slightly larger sized (9 cm^2) zinc plate was mounted in the cell, resulting in smaller zinc overpotentials as can be seen in the 1400 h inlet in Figure 1. However, zinc dendrites were visibly growing on the edges of the new zinc electrode, whereas the middle, directly opposite the air electrode, was slowly depleted. There were no short-circuits because of the distance of 2 cm between air and zinc electrode. As the small flow cell set-up was open on the top, repeated renewing of the zinc electrode without complete disassembly of the cell was possible.

Regarding the air electrode, its surface exhibited initially high hydrophobicity, so that it was kept in electrolyte for 1 h prior to operation. Nevertheless, an "activation" behavior was visible within the first 50 h of operation as can be seen in the first inlet of Figure 1 and in Figure 2. The separate referencing of air, zinc and cell potentials allowed for better attribution of the effects occurring within the cell. For example, the cell voltage often decreased within one discharge cycle, which can rather be ascribed to increasing zinc electrode potential than to the air electrode, which in fact, exhibited slightly improving ORR potential within the 1 h discharge during each cycle.

After about 400 h of operation the electrolyte had a slightly orange color, indicating carbon corrosion to a certain degree,^[10] but no further change of color was observed thereafter (see image in the supporting information Figure S9). Also, inwards bulging of the air electrode caused by the 10–15 mbar pressure from the immersed gas exhaust became apparent over time, leading to small electrolyte leakage between electrode's edges

and the softened polymeric sealing after about 750 h (shown in Figure S1 in the supporting information). Initially, small droplets were taken out with the air flow, however, after 1000 h of operation the effect became more pronounced. In combination with slowly declining hydrophobicity, this resulted finally in decreasing discharge performance with the ORR potential dropping below 1.0 V after 1250 h (560 cycles) and to the end of testing after 1800 h.

After 1800 h the air electrode was washed on both sides with pure KOH (with no ZnO) and with deionized water in order to remove any precipitates (carbonates, ZnO, hydroxides^[34,35]) within the electrode. Although no crystallized deposits were visible, the high ORR performance was not restored by that procedure. This is mainly attributed to the degraded hydrophobicity of the electrode^[14] as shown in Figure 7.

2.3. Electrochemical Characterization of 50 cm² Air Electrode E2

In an up-scaled zinc-air flow cell set-up, a 50 cm² air electrode (E2) was mounted together with a 7×8 cm sized copper plate which was priorly coated with about 0.5 g of electrodeposited zinc in order to reduce the zinc corrosion problem encountered in the small cell and to prevent contact loss at the clamping. As in the small set-up, the cell voltage as well as both half-cell potentials were measured. The air electrode was actively supplied with air from a compressor and the air exhaust immersed in 15 cm of water. As a result of the smaller in- and outlets of this cell, only lower electrolyte flow rates of 2 cm s⁻¹ were possible.

The result of the long-term cycling measurement of this zinc-air flow cell employing E2 is shown in Figure 3 and the course of the air electrode potentials in Figure 4b. Because of the current restrictions of the potentiostat, the pulse charging was – compared to E1 – performed at half the current density (50 mA cm⁻² pulse) but double the time length (2 h instead of 1 h; 3 h overall cycle length). The successfully up-scaled zinc-air flow battery was operated for 320 h (92 cycles). Similar performances to the small E1 cell were obtained, as a comparison of the two 100 h inlets of Figure 1 and Figure 3 shows. E2 also

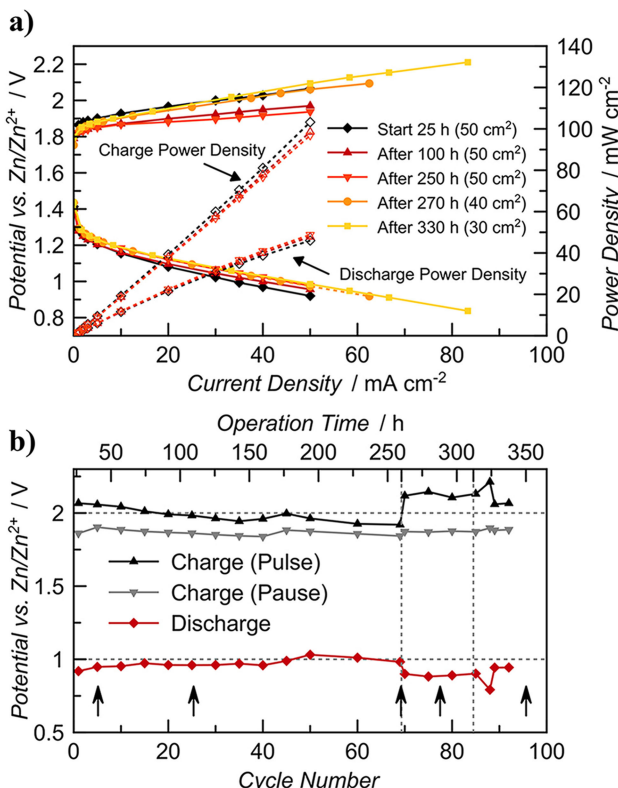


Figure 4. Characterization of 50 cm² air electrode E2 showing a) polarization curves measured for ORR and OER including the power density of the air electrode needed for charging and obtained during discharge (dashed lines) and b) maximum and minimum potentials during pulse charging (50 mA cm⁻² pulse for 50 ms, 50 ms pause) and the ORR potentials (black arrows indicate the breaks for recording polarization curves and EIS, the dashed vertical lines the twotimes the cell had to be opened).

exhibited the same “activation” effect with gradually improving performance at the beginning of operation. As shown in the first inlet of Figure 3, within the first 10 h of the measurement the current density was slowly increased up to 30 mA cm⁻² (20 min cycles) in order to minimize degradation effects by uneven current distributions. Only after that it was raised to 50 mA cm⁻². After the first 50 h of operation, the potential course of the air electrode shows similar charge/discharge

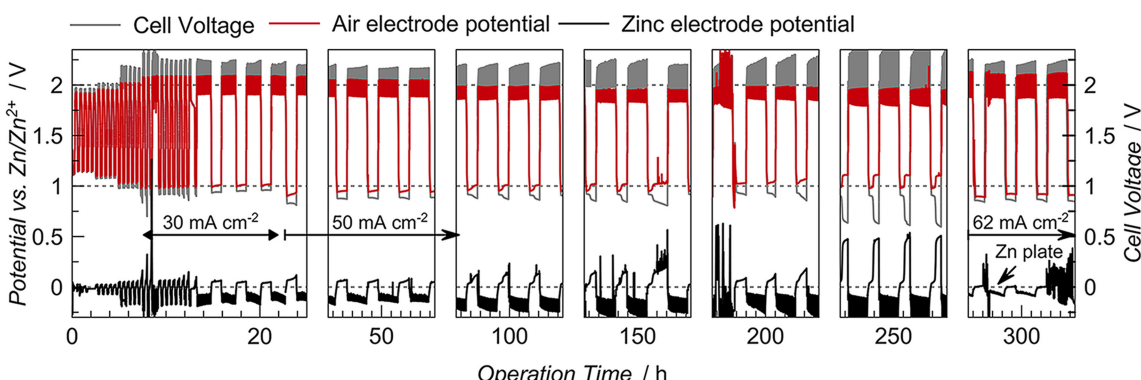


Figure 3. Electrochemical long-term charge/discharge cycling of a zinc-air flow cell with 50 cm² bifunctional air electrode (E2) operated at 50 mA cm⁻² (air) with pulse charging (50 mA cm⁻² pulse), actively supplied with air at RT and with flowing 8 M KOH + 0.5 M ZnO electrolyte (2 cm s⁻¹ surface flow velocity).

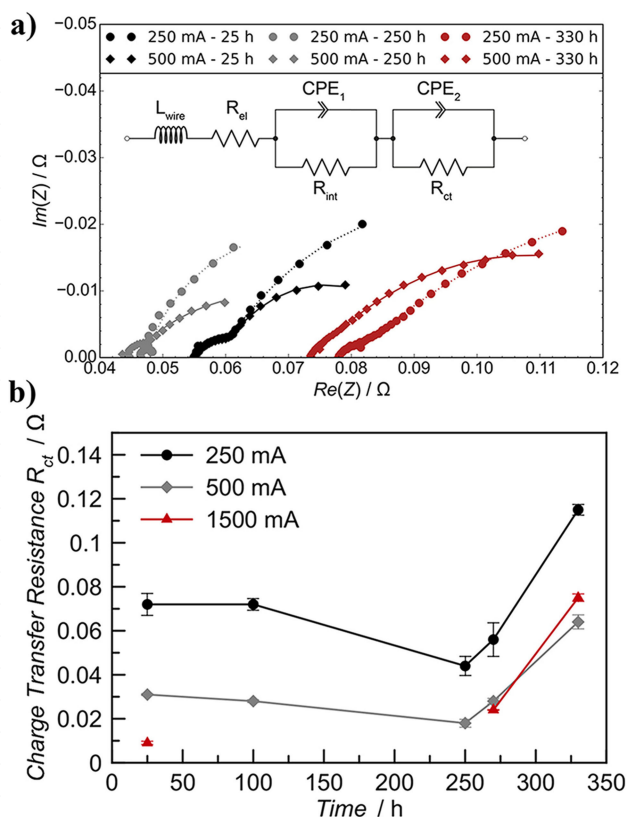


Figure 5. EIS measurements at OER of 50 cm^2 air electrode E2 showing a) Nyquist plots at different currents (● 250 mA, ◆ 500 mA, ▲ 1500 mA, – 25 h, – 250 h, – 330 h). The different electrolyte resistances arise due to the replacement of the copper plate with a zinc plate. At the top the equivalent circuit used for fitting the OER and ORR spectra, respectively, is pictured. The line plots are the fitting results of the equivalent circuit (see Table S4 in supporting information). b) The trend of the charge transfer resistance R_{ct} at different currents and times (● 250 mA, ◆ 500 mA, ▲ 1500 mA).

potentials as E1 with the ORR at $\sim 1.0 \text{ V}$ and the pulse charging $< 2.0 \text{ V}$ vs. Zn/Zn^{2+} as depicted in Figure 4b.

To gain further insight into the mechanisms within the up-scaled cell, polarization curves (depicted in Figure 4a) as well as impedance spectra (Figure 5 and Figure 6) were recorded. In the polarization curves the ORR and OER kinetic activation region up to 5 mA cm^{-2} and the linear ohmic region are visible.

The corresponding power densities show the very high losses caused by the overpotentials of ORR and OER. Double the charging power is required as is regained during discharge. Further potentials values and ΔV of the polarization curves are listed in Table S3 in the supporting information.

Electrochemical impedance spectroscopy (EIS), shown in Figure 5 for OER and Figure 6 for ORR, revealed that the charge transfer resistance, R_{ct} , which represents the kinetics of the OER and ORR, respectively,^[36–39] followed the same behavior as the overpotentials and the trend of the potentials depicted in Figure 4. In case of OER, R_{ct} slightly decreased within the first 250 h (see Figure 5b), which indicates that the kinetics of the OER was improved and therefore the overpotential dropped. Reasons can be the good transport of product water away from the air electrode, through the still very hydrophobic structure. Because of the improved wetting within the electrode, more

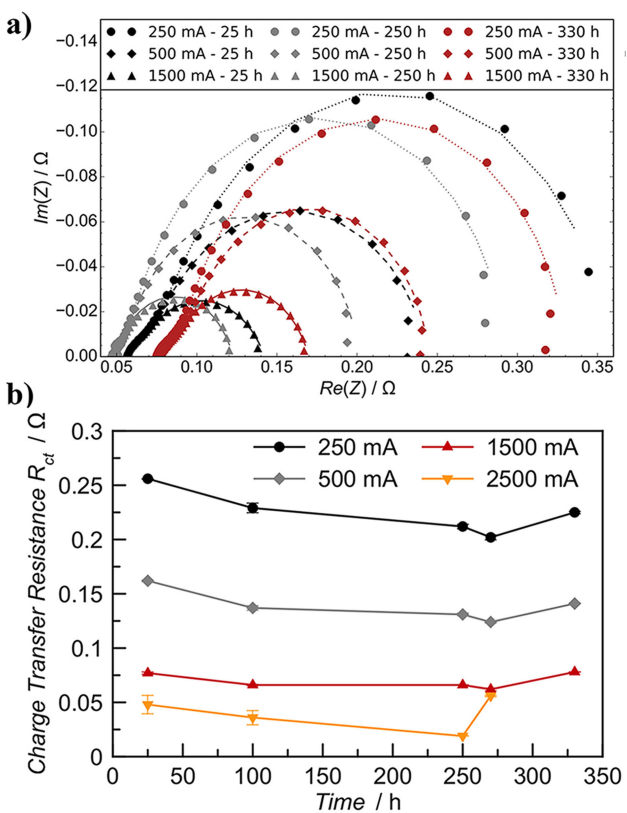


Figure 6. EIS measurements at ORR of 50 cm^2 air electrode E2 showing a) Nyquist plots at different currents (● 250 mA, ◆ 500 mA, ▲ 1500 mA, – 25 h, – 250 h, – 330 h, fitting results in Table S5 in supporting information) and b) the trend of the R_{ct} at different times and currents (● 250 mA, ◆ 500 mA, ▲ 1500 mA, ▽ 2500 mA).

active sites at the catalyst were available.^[38] This corresponds well with the decreasing ΔV measured for E2 within this 250 h as depicted in Figure 4b. Further interpretation of the EIS data can be found in the supporting information in Figures S3–S6 and Tables S4 and S5.

Due to the long recording times and the applied constant charging current (no pulse charging) during the measurement of the polarization curves ($\sim 2 \text{ h}$) as well as the EIS ($\sim 5 \text{ h}$) each time, the zinc deposited unevenly on the copper current collector plate, which resulted in ever higher overpotentials after 100 h (visible in Figure 3 between 50–250 h). In consequence, copper was open to electrolyte and an oxidation peak on the zinc electrode and a reduction peak on the air electrode side became more and more apparent, which is attributed to Cu oxidation and reduction in the highly alkaline media resulting in mixed potentials.^[40–42] The effect became so pronounced (see 250 h inlet in Figure 3) that the cell had to be completely disassembled (see image in Figure S2 in the supporting information) and a new zinc plate ($7 \times 8 \text{ cm}$) was implemented. Thereby the air electrode was slightly damaged but could be resealed (new surface area 40 cm^2).

After reassembly the measurements were continued but although the ORR performance stayed the same the charging potential significantly increased. EIS confirmed a significant increase of R_{ct} after reassembly, as depicted in the Figure 5b,

resulting in slower kinetics of the OER and higher overpotentials. This behavior can be attributed to residual hydroxides, ZnO and carbonates precipitated in the emptied cell during maintenance as a drying period after resealing was necessary.^[43] Looking at R_{ct} of the ORR, it is also in good accordance with the results presented in Figure 4. Within the first 250 h values of R_{ct} were nearly unchanged, but after disassembly the resistance increased like in the OER case (see Figure 6b). These results support the hypothesis that precipitates are the cause for the lack of performance at the end as the maintenance interval severely disrupted the balance within the air electrode. After 312 h, due to problems with the zinc half-cell potential measurement, a second disassembly and reassembly was done whereby the sealing around the air electrode had to be renewed, which reduced the open area to 30 cm². A last set of polarization curves and impedance spectra were recorded, but because of zinc deposits on the Luggin capillary as well as leakages at the edges of the air electrode including dry-out at the gas inlet as shown in supporting information Figure S9, the measurement was stopped.

The aforementioned changes in hydrophobicity over the course of long-term operation are also visible in Figure 7, where three light microscopy images and three photographs of a new electrode, of E2 after 330 h of operation and of E1 after 1800 h of operation are shown. It is clear that the hydrophobicity gradually decreases although the structure of the electrode does not appear to be altered significantly. Whereas the electrolyte droplets readily pearly off the new electrode, the droplets on E2 – although still defined after 320 h of operation – already slightly soaked into the electrode. After 1800 h of operation (E1), the soaking effect is most severe, while the fine structure of the carbon fibers appears primarily unchanged. On perovskite as well as carbon-based catalysts the ORR proceeds to some degree via the two electron pathway, whereby H₂O₂ is formed as the intermediate product.^[10,21,24] A reason for PTFE degradation can hence be attributed to H₂O₂ or HO[•] radical attack of the F–C chain, an effect known from PEM fuel cells.^[44,45]

2.4. Electrochemical Characterization of 55 cm² Air Electrode E3

As the constant charging currents during recording of polarization curves and electrochemical impedance spectra resulted in unstable zinc potentials, a new air electrode (E3; 55 cm² sized) was mounted in the up-scaled flow set-up. As zinc electrode, a new zinc plate was utilized with a copper current collector soldered on the backside of the plate. The continuous long-term cycling measurement of the zinc-air cell with air electrode E3 at increasing current densities is depicted in Figure 8, showing stable cell voltages as well as half-cell potentials over a duration of 130 h and 48 cycles. The obtained air electrode performance during pulse charging and discharge is comparable to E1 and E2 and even after 120 h a slight improvement in the air electrode's performance was observed as summarized in Table 1. In contrast to this, the zinc electrode

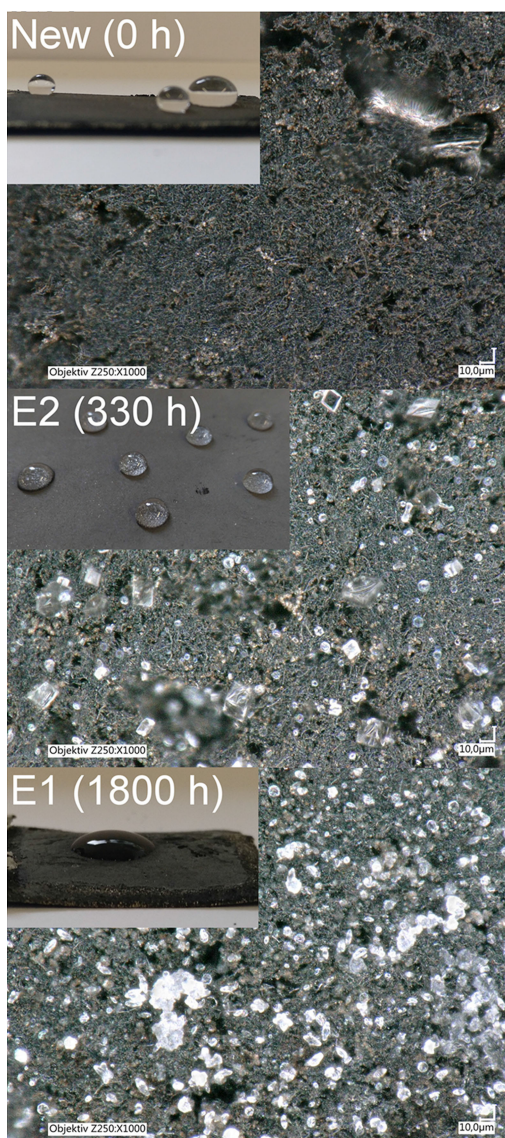


Figure 7. Light microscopy images and photographs (left upper corners) of the electrolyte facing side of a new electrode and E2 and E1 after operation depicting the change in hydrophobicity. Also, ZnO and electrolyte residues, which could not be completely removed by washing, are visible as white deposits. Images of the air supplied side are shown in Figure S7 in the supporting information.

showed increasing overpotentials over time, which can be attributed to uneven zinc deposition over the whole zinc plate surface area with agglomeration of zinc on the lower part. This was probably caused by the lower flow rates of 2 cm s⁻¹. Higher flow-rates as used in the small set-up are thus preferable and can result in a prolonged cycle life of the zinc electrode.

After 130 h the measurement was stopped for a few days but restarting of the cell was prevented by too severe zinc corrosion and thus leakage of the cell on the side of the zinc electrode (probably accelerated by corrosion currents between zinc and copper current collector). Nevertheless, very good and stable potentials for the bifunctional air electrode were obtained even at high current densities of 50 mA cm⁻², showing the feasibility of the manufacturing process for larger-sized

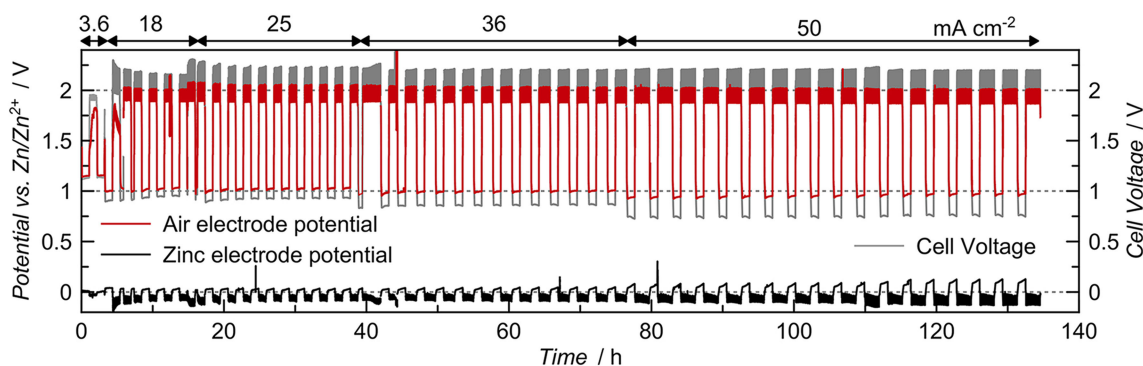


Figure 8. Electrochemical long-term charge/discharge cycling of a zinc-air flow cell with 55 cm^2 bifunctional air electrode (E3) operated up to 50 mA cm^{-2} (air) with pulse charging (50 mA cm^{-2} pulse), actively supplied with air at RT and with flowing $8 \text{ M KOH} + 0.5 \text{ M ZnO}$ electrolyte (2 cm s^{-1} surface flow velocity). Fluctuations within the first 5 h of operation were caused by slight blockage of the air electrode's Luggin capillary.

Table 1. Potentials obtained during long-term charge/discharge cycling up to 50 mA cm^{-2} discharge of the zinc-air flow cell with 55 cm^2 air electrode E3.

	Potentials at 25 mA cm^{-2} (37 h)/V			Potentials at 36 mA cm^{-2} (75 h)/V			Potentials at 50 mA cm^{-2} (132 h)/V		
	OER ^[a]	ORR	ΔV	OER ^[a]	ORR	ΔV	OER ^[a]	ORR	ΔV
Cell Voltage	2.10	0.93	1.17	2.08	0.86	1.22	2.07	0.75	1.32
Air vs. Zn/Zn ²⁺	1.97	1.04	0.93	1.95	1.01	0.94	1.94	0.97	0.97
Zinc vs. Zn/Zn ²⁺	-0.06	0.03	0.09	-0.06	0.05	0.11	-0.08	0.13	0.21

[a] Mean value between pulse potential and pause potential (duty cycle $\gamma = 0.5$)

electrodes. The high catalytic activity toward ORR/OER of the $\text{La}_{0.6}\text{Sr}_{0.4}\text{Co}_{0.2}\text{Fe}_{0.8}\text{O}_3$ perovskite could be successfully transferred from the small electrode to over ten times larger sized electrodes (i.e. $50\text{--}55 \text{ cm}^2$).

3. Conclusions

In this work, long-term operation of bifunctional air electrodes catalyzed with highly stable $\text{La}_{0.6}\text{Sr}_{0.4}\text{Co}_{0.2}\text{Fe}_{0.8}\text{O}_3$ perovskite were demonstrated for application in stationary zinc-air flow batteries. In a small set-up of 4 cm^2 a durability of 1000 h and an overall operation time of 1800 h with high voltage efficiencies of the air electrode of $>50\%$ at 50 mA cm^{-2} over 700 cycles were achieved. The scale-up of the air electrode was successfully performed, and 50 and 55 cm^2 air electrodes were operated in an up-scaled flow set-up for 320 h and 130 h, respectively. They achieved similar charge and discharge performances and the same characteristic trends were observed in the small and in the bigger cell, respectively. Thereby, separate referencing of the half-cell as well as the cell potentials was essential for distinguishing the effects within the cell. Electrochemical impedance spectroscopy of the air electrode was applied for obtaining knowledge of the mechanisms within the electrode, whereby two distinctive processes could be distinguished. One is attributed to the interface of the solid to the electrolyte; the other one is related to the kinetics of the overall OER or ORR reaction. Looking closer at the latter, the charge transfer resistance for ORR and OER, respectively, decreased slightly within the first 250 h of operation, leading to a better performance of the battery and to lower over-

potentials. This can be attributed to a slowly changing hydrophobicity and thus an improved wetting of the electrode. After disassembly, the charge transfer resistance for ORR and OER increased significantly probably because of precipitation of ZnCO_3 or ZnO within the electrode during the maintenance, leading to a weak performance and to higher overpotentials.

Regarding end-of-life, especially of the small air electrode, changes in hydrophobicity primarily on the electrolyte facing side by PTFE degradation^[10] was found to be the main cause of initially slowly improving (about first 50 h) but then gradually decreasing ORR performance. Because of the rather low charging potentials of below 2.0 V, carbon corrosion was minimized in this current density range as the nearly colorless electrolyte proved and also the catalyst itself exhibited high stability throughout repeated cycling in this broad potential range. Thus, further optimization has to be tackled in regard to the hydrophobic binder material.

The zinc-air flow cell is a highly sensitive cell system, where the operation conditions have to be selected carefully and the disruption through, for example, maintenance minimized. Although many problems could be suppressed with flowing electrolyte, inhomogeneous zinc morphology proved to be a major challenge, especially in the up-scaled cell under the conditions of long-term operation of a few hundred hours. This work mainly focused on the optimization of the air electrode, however, for further studies investigations on improving the zinc electrode have to be done by applying the methods, which were recently summarized by Mainar et al.^[35] and Turney et al.^[46] Changing to a horizontal flow set-up^[14,17] is another way to tackle some of these issues. In addition, electrochemical engineering becomes more and more important the larger the

unit-cell,^[5] and is especially important when operating a stack. Changes in electrolyte conductivity and density have to be monitored^[47–49] and maintenance intervals minimized in order to circumvent the issues related to dry-out and sealing of the cell, which were the main cause of decreasing performance of the larger-sized air electrodes.

Experimental Section

All chemicals were used as purchased without further purification. Commercial $\text{La}_{0.6}\text{Sr}_{0.4}\text{Co}_{0.2}\text{Fe}_{0.8}\text{O}_3$ perovskite (LSCF; surface area 10–14 m^2g^{-1} , size $d_{50}=0.4\text{--}0.8\text{ }\mu\text{m}$; Sigma-Aldrich) was homogeneously dispersed on carbon nanofibers (CNF; HTF150FF-LHT (lowheat), 70–150 nm diameter, >10 μm length, heat-treated at 1000 °C, resistance <10⁻³ Ωcm^{-1} , metal impurities <0.5 wt.%, N₂ specific surface area 43 m^2g^{-1} , Electrovac AG, Austria) in a weight ratio of 3:1 in ultra-pure water/2-propanol 1:1 (200 mL for 5 g of LSCF/CNF) for 1 h using an ultrasonic probe (UP400 S; Hielscher, Germany). The solvent was slowly evaporated at 80 °C under vigorous stirring and the dry powder ground in a mortar (see SEM images in Figure S8 in the supporting information). Two separate electrode pastes were prepared using about 1–1.5 g per 25 cm^2 electrode area. Paste one contained 45 wt% LSCF/CNF, 40 wt% Ni powder (Type 255, 2.2–2.8 μm particle size; Novamet Specialty Products Corp., USA) and 15 wt% PTFE (Dispersion TF5135 GZ; 58 wt%, 5.5 wt% emulsifier, 190 nm; 3 M Dyneon) and paste two 85 wt% LSCF/CNF and 15 wt% PTFE. The pastes were separately mixed in ultra-pure water/2-propanol 1:1 (about 10 mL per g paste) until a dough-like consistency was obtained. They were spread on opposite sides of nickel foam (thickness 1.6 mm, pore size 450 μm , area density 420 g m^{-2} ; Alantum Corporation, Germany), dried overnight and sinter-pressed at 150 kg cm^{-2} for 20 min at 300 °C. The final catalyst loading was about 40 mg cm^{-2} LSCF.

Electrochemical characterization was performed using a custom-made vertical flow-cell set-up with a DC centrifugal pump (WPDC-02.5 L-1.00 M-12-VP; Rotek, Austria) with either a 0.5 L or 1 L electrolyte reservoir for the 4 cm^2 cell (E1) or the 50 cm^2 (E2)/55 cm^2 (E3) cell, respectively. As electrolyte 8 M KOH (>85% pellets; Carl Roth GmbH + Co.KG) with 0.5 M ZnO (99.99%; Alfa Aesar) was utilized, which was pumped from bottom to top with an electrode surface flow velocity of 8 cm s^{-1} in the small set-up and 2 cm s^{-1} in the big set-up. Assuming zincate concentrations of 0.5 M (discharged) and 0.2 M charged, this cell has a nominal capacity of about 16 Ah (see calculations in the supporting information). The air electrodes were always operated in three-electrode mode using the air electrode as working electrode, a zinc plate (E1 and E3) or zinc-plated copper plate (E2) as counter electrode and a zinc foil (1.6 mm thickness, AlfaAesar) as reference electrode, which was mounted in front of the air electrode via a Luggin capillary. In addition, the cell voltage between zinc and air electrode as well as the zinc electrode potential via a second zinc foil reference Luggin capillary set in front of the zinc electrode, were recorded. The distance between air and zinc electrode was in both set-ups 2 cm. All current densities mentioned in this work are in respect to the open surface area of the air electrode to the electrolyte. The backside of the electrode was actively supplied with air from a compressor (25 mL min^{-1} for the 4 cm^2 and 350 mL min^{-1} for 50 cm^2 /55 cm^2 sized electrode). It contained ambient CO₂ and was not humidified. The gas exhaust was immersed in 10–15 cm of water to counter the hydrostatic pressure of the electrolyte. For more details, images of the cells and the set-up can be found in the supporting information (Figure S1 and Figure S2).

Cycling experiments for the 4 cm^2 electrode E1 comprised 1 h charge and 1 h discharge (2 h per cycle) performed with a BaSyTec Cell Test System (CTS Lab) with corresponding software at 50 mA cm^{-2} (mean) with additional pulse charging at 100 mA cm^{-2} during a 50 ms pulse and no current during 50 ms pause (duty cycle $\gamma=0.5$, 36,000 pulses per hour). Because of the current restriction of 3 A of the potentiostat the pulse charging times were prolonged for the larger sized electrodes accordingly to match the discharge capacity of 1 h (for example 2 h pulse charging at 25 mA cm^{-2} (mean) with 50 mA cm^{-2} pulses with $\gamma=0.5$, then 1 h discharge at 50 mA cm^{-2}). Polarization curves were recorded in galvanostatic mode with 5 min steps. Electrochemical impedance spectroscopy was performed in three-electrode mode with the air electrode as working electrode on an IM6ex and a PP240 potentiostat (Zahner Elektrik) between 50 mHz and 10 kHz at 250 mA, 500 mA and 1500 mA for OER and –250 mA, –500 mA, –1500 mA and –2500 mA for ORR (three impedance measurements at each step) with amplitudes of 50–200 mA. For E2 the currents during EIS were kept the same although the surface area of the air electrode was decreased from 50 cm^2 to 40 and 30 cm^2 . Light microscopy was performed on a Keyence VHX-S500E.

Acknowledgements

Funding by the Austrian Federal Ministry of Transport, Innovation and Technology (BMVIT) and The Austrian Research Promotion Agency (FFG) through the program “e!MISSION.at Energieforschungsprogramm” (No. 848933) is gratefully acknowledged. We also want to thank our cooperation partners from the Institute of Chemistry and Technology of Materials at Graz University of Technology and our industry partners VARTA Micro Innovation GmbH (Austria). Special thanks go to our cooperation partner Hans-Jürgen Pauling from the German company RECAT GmbH for developing and providing the large-scale test cell.

Conflict of Interest

The authors declare no conflict of interest.

Keywords: bifunctional air electrode • $\text{La}_{0.6}\text{Sr}_{0.4}\text{Co}_{0.2}\text{Fe}_{0.8}\text{O}_3$ perovskite • oxygen evolution reaction • oxygen reduction reaction • zinc-air flow batteries

- [1] P. Alotto, M. Guarneri, F. Moro, *Renewable Sustainable Energy Rev.* **2014**, 29, 325–335.
- [2] J. Cho, S. Jeong, Y. Kim, *Prog. Energy Combust. Sci.* **2015**, 48, 84–101.
- [3] G. L. Kyriakopoulos, G. Arabatzis, *Renewable Sustainable Energy Rev.* **2016**, 56, 1044–1067.
- [4] L. F. Arenas, A. Loh, D. P. Trudgeon, X. Li, C. Ponce de León, F. C. Walsh, *Renewable Sustainable Energy Rev.* **2018**, 90, 992–1016.
- [5] L. F. Arenas, C. Ponce de León, F. C. Walsh, *J. Energy Storage* **2017**, 11, 119–153.
- [6] B. R. Chalamala, T. Soundappan, G. R. Fisher, M. R. Anstey, V. V. Viswanathan, M. L. Perry, *Proc. IEEE* **2014**, 102, 1–24.
- [7] A. Khor, P. Leung, M. R. Mohamed, C. Flox, Q. Xu, L. An, R. G. A. Wills, J. R. Morante, A. A. Shah, *Mater. Today Energy* **2018**, 8, 80–108.
- [8] P. K. Leung, T. Martin, A. A. Shah, M. R. Mohamed, M. A. Anderson, J. Palma, *J. Power Sources* **2017**, 341, 36–45.
- [9] M. Park, J. Ryu, W. Wang, J. Cho, *Nat. Rev. Mater.* **2017**, 2, 16080.
- [10] E. Davari, D. G. Ivey, *Sustain. Energy Fuels* **2018**, 2, 39–67.

- [11] J. Fu, Z. P. Cano, M. G. Park, A. Yu, M. Fowler, Z. Chen, *Adv. Mater.* **2017**, *29*, 1604685.
- [12] X. Han, X. Li, J. White, C. Zhong, Y. Deng, W. Hu, T. Ma, *Adv. Energy Mater.* **2018**, *8*, 1801396.
- [13] J. Pan, Y. Y. Xu, H. Yang, Z. Dong, H. Liu, B. Y. Xia, *Adv. Sci.* **2018**, *5*, 1700691.
- [14] P. Pei, K. Wang, Z. Ma, *Appl. Energy* **2014**, *128*, 315–324.
- [15] M. Xu, D. G. Ivey, Z. Xie, W. Qu, *J. Power Sources* **2015**, *283*, 358–371.
- [16] B. Amunátegui, A. Ibáñez, M. Sierra, M. Pérez, *J. Appl. Electrochem.* **2018**, *48*, 627–637.
- [17] M. Bockelmann, U. Kunz, T. Turek, *Electrochem. Commun.* **2016**, *69*, 24–27.
- [18] Y. Li, M. Gong, Y. Liang, J. Feng, J.-E. Kim, H. Wang, G. Hong, B. Zhang, H. Dai, *Nat. Commun.* **2013**, *4*, 1805.
- [19] W. T. Hong, M. Risch, K. A. Stoerzinger, A. Grimaud, J. Suntivich, Y. Shao-Horn, *Energy Environ. Sci.* **2015**, *8*, 1404–1427.
- [20] D. Pletcher, X. Li, S. W. T. Price, A. E. Russell, T. Sönmez, S. J. Thompson, *Electrochim. Acta* **2016**, *188*, 286–293.
- [21] D. Chen, C. Chen, Z. M. Baiyee, Z. Shao, F. Ciucci, *Chem. Rev.* **2015**, *115*, 9869–9921.
- [22] K. Elumeeva, J. Masa, J. Sierau, F. Tietz, M. Muhler, W. Schuhmann, *Electrochim. Acta* **2016**, *208*, 25–32.
- [23] J.-I. Jung, M. Risch, S. Park, M. G. Kim, G. Nam, H.-Y. Jeong, Y. Shao-Horn, J. Cho, *Energy Environ. Sci.* **2016**, *9*, 176–183.
- [24] Y. Zhu, W. Zhou, Z. Shao, *Small* **2017**, *13*, 1603793.
- [25] S. Müller, O. Haas, C. Schlatter, C. Cominellis, S. Mu, *J. Appl. Electrochem.* **1998**, *28*, 305–310.
- [26] J. Pan, L. Ji, Y. Sun, P. Wan, J. Cheng, Y. Yang, M. Fan, *Electrochim. Commun.* **2009**, *11*, 2191–2194.
- [27] K. Wang, P. Pei, Y. Wang, C. Liao, W. Wang, S. Huang, *Appl. Energy* **2018**, *225*, 848–856.
- [28] H. E. Lin, C. H. Ho, C. Y. Lee, *Surf. Coat. Technol.* **2017**, *319*, 378–385.
- [29] B. Pichler, B. S. Berner, N. Rauch, C. Zelger, H. J. Pauling, B. Gollas, V. Hacker, *J. Appl. Electrochem.* **2018**, *48*, 1–14.
- [30] C. Zelger, J. Laumen, A. Laskos, B. Gollas, *Electrochim. Acta* **2016**, *213*, 208–216.
- [31] Z. P. Cano, M. G. Park, D. U. Lee, J. Fu, H. Liu, M. W. Fowler, Z. Chen, *J. Phys. Chem. C* **2018**, *122*, acs.jpcc.8b06243.
- [32] B. Pichler, S. Weinberger, L. Reščec, I. Grimmer, F. Gebetsroither, B. Bitschnau, V. Hacker, *Electrochim. Acta* **2017**, *251*, 488–497.
- [33] X. Li, D. Pletcher, A. E. Russell, F. C. Walsh, R. G. A. Wills, S. F. Gorman, S. W. T. Price, S. J. Thompson, *Electrochim. Commun.* **2013**, *34*, 228–230.
- [34] J.-F. Drilllet, F. Holzer, T. Kallis, S. Müller, V. M. Schmidt, *Phys. Chem. Chem. Phys.* **2001**, *3*, 368–371.
- [35] A. R. Mainar, L. C. Colmenares, J. A. Blázquez, I. Urdampilleta, *Int. J. Energy Res.* **2018**, *42*, 903–918.
- [36] D. U. Lee, J. Y. Choi, K. Feng, H. W. Park, Z. Chen, *Adv. Energy Mater.* **2014**, *4*, DOI 10.1002/aenm.201301389.
- [37] D. Thiele, A. Züttel, *J. Power Sources* **2008**, *183*, 590–594.
- [38] Z. Chen, A. Yu, D. Higgins, H. Li, H. Wang, Z. Chen, *Nano Lett.* **2012**, *12*, 1946–1952.
- [39] H. Arai, S. Müller, O. Haas, *J. Electrochem. Soc.* **2000**, *147*, 3584.
- [40] S. Dong, Y. Xie, G. Cheng, *Electrochim. Acta* **1992**, *37*, 17–22.
- [41] W. Z. Le, Y. Q. Liu, *Sensors* **2009**, *141*, 147–153.
- [42] W. Z. Teo, A. Ambrosi, M. Pumera, *Electrochim. Commun.* **2013**, *28*, 51–53.
- [43] M. Prabu, P. Ramakrishnan, H. Nara, T. Momma, T. Osaka, S. Shanmugam, *ACS Appl. Mater. Interfaces* **2014**, *6*, 16545–16555.
- [44] R. Borup, J. Meyers, B. Pivovar, Y. S. Kim, R. Mukundan, N. Garland, D. Myers, M. Wilson, F. Garzon, D. Wood, *Chem. Rev.* **2007**, *107*, 3904–3951.
- [45] C. Zhou, M. A. Guerra, Z. M. Qiu, T. A. Zawodzinski, D. A. Schiraldi, *Macromolecules* **2007**, *40*, 8695–8707.
- [46] D. E. Turney, J. W. Gallaway, G. G. Yadav, R. Ramirez, M. Nyce, S. Banerjee, Y. C. K. Chen-Wiegart, J. Wang, M. J. D'Ambrose, S. Kolhekar, *Chem. Mater.* **2017**, *29*, 4819–4832.
- [47] R. J. Gilliam, J. W. Graydon, D. W. Kirk, S. J. Thorpe, *Int. J. Hydrogen Energy* **2007**, *32*, 359–364.
- [48] A. Gavrilović-Wohlmuther, A. Laskos, C. Zelger, B. Gollas, A. Harding Whitehead, *J. Energy Power Eng.* **2015**, *9*, 1019–1028.
- [49] G. Li, K. Zhang, M. A. Mezaal, R. Zhang, L. Lei, *Int. J. Electrochem. Sci.* **2015**, *10*, 6672–6683.

Manuscript received: September 14, 2018

Accepted Article published: October 18, 2018

Version of record online: October 31, 2018